Effects of diffusion on magnetic resonance imaging of laser-polarized xenon gas

Yi-Qiao Song, Boyd M. Goodson, Bhima Sheridan, Thomas M. de Swiet, and Alexander Pines
Materials Sciences Division, Lawrence Berkeley National Laboratory and Department of Chemistry, University of California, Berkeley, California 94720

(Received 23 September 1997; accepted 15 January 1998)

Molecular diffusion during the application of magnetic field gradients can distort magnetic resonance images. A systematic characterization of these distortions in one dimension was performed using highly spin-polarized xenon gas. By varying the strength of the applied gradient and the geometric dimension of the sample, the evolution of these image distortions between the regimes of strong and weak diffusion was observed. These results are compared with numerical simulations. By directly measuring the displacement distribution of the polarized xenon atoms, it is shown that in the weak-diffusion regime the image distortions originate from the restricted diffusive motion near the sample boundaries, in agreement with previous theoretical work. Additionally, it is shown that the effects of diffusion can be utilized to enhance the contrast between the boundaries and bulk in the images of polarized gas samples, and thus may be exploited as a means of boundary detection in such systems. © *1998 American Institute of Physics.* [S0021-9606(98)02915-8]

I. INTRODUCTION

MRI (magnetic resonance imaging) has been widely utilized in medicine as an informative diagnostic tool,[1] and the recent development of using highly spin-polarized noble gases as contrast agents for human lung imaging[2–6] has stimulated considerable interest. However, one limitation on the resolution of ''polarized'' gas imaging is due to the rapid diffusion of gases, typically several orders of magnitude higher than in liquids. Currently, the highest spatial resolution achieved using gas-phase MRI is $\sim 100\ \mu$m; this resolution was obtained in a phantom sample of polarized xenon[7] and was primarily determined by the fast diffusion of the gas and the strength of the magnetic field gradients used in the experiments.

In addition to limiting the MRI resolution, diffusion may distort the line shape of MR images for samples containing boundaries or diffusion barriers within the space being imaged. This was first suggested by numerical simulations[8,9] and was later explored experimentally[10,11] using ^{1}H NMR. In one dimension, the diffusion problem can be solved analytically.[12–14] However, it has been difficult to experimentally characterize such effects in detail using ^{1}H NMR. Given a value for the diffusion constant of water molecules $D_w \approx 2\times 10^{-5}$ cm^2/s, the corresponding effects from diffusion would occur over a distance $d=\sqrt{2D_w t}$, or less than 10 μm during a time t of a typical one-dimensional (1D) imaging experiment (~ 10 ms). An imaging resolution below 10 μm is difficult to achieve because the signal from such a small region is generally too weak.

The use of polarized xenon gas for such studies provides two advantages: a strong NMR signal and a large diffusion length. Given the xenon diffusion constant at 1 atm of 0.0565 cm^2/s,[15] one obtains a value of $d=0.034$ cm for $t=10$ ms, which can be readily measured. Recently Saam *et al.*[16] used samples of polarized ^{3}He to study the the effects of diffusion on imaging, while demonstrating the ability to image such polarized gases at low field (3.1 mT); those investigations were performed in the weak-diffusion regime, where the diffusion length is much smaller than the sample size. Recently, Schmidt *et al.*[17] used laser-polarized ^{3}He to study gas diffusion at high field (1.9 T).

In this paper, we characterize the effects of diffusion on MRI in a 1D sample at a magnetic field of 4.3 T using polarized xenon gas. Our results show a smooth evolution of the MR images from the regime of complete motional averaging to a regime where the image distortions due to diffusion are present only at the edges. We also show that these edge effects originate from the partially restricted diffusion at the sample boundaries by directly measuring the displacement distribution. Finally, we show results from diffusion-weighted imaging experiments that actively enhance these edge effects in order to demonstrate boundary detection. These results agree well with previous theoretical and experimental work.

II. MATERIALS AND METHODS

A long rectangular glass tube (0.07 by 0.66 cm in cross-section) was used for all experiments, and is shown in Fig. 1. Attached above the sample tube is a spherical xenon reservoir (not shown); the xenon pressure was typically about 2 atm. The tube was placed in the probe parallel to the direction ($\mathbf{z}$) of the static magnetic field (B_0). We designate the direction along the 0.66 cm side to be $\mathbf{x}$, and the 0.07 cm side to be $\mathbf{y}$. 1D imaging experiments were performed along both $\mathbf{x}$ and $\mathbf{y}$. In all experiments, a slice-selection $\mathbf{z}$ gradient was applied during the rf excitation, creating a slice depth of about 0.4 cm. The rf coil was a saddle coil 2.0 cm long and 1.2 cm in diameter. The large size of the coil and the slice

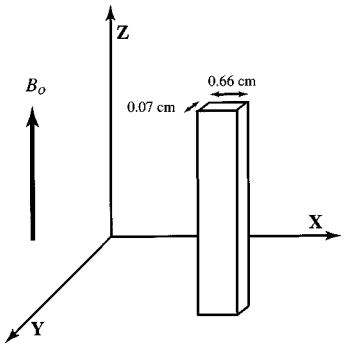

FIG. 1. Geometry of the sample used in the experiments and the definition of the coordinate system. The **z** axis is defined to be parallel to the external magnetic field (B_0), while the **x** and **y** axes are defined in the text.

selection were used to ensure a homogeneous rf field at a significant cost in filling factor. Because the effects of diffusion are most pronounced at low field gradient and directly manifest themselves as changes in the spectral line shape, it was important to obtain a homogeneous static field in the absence of the imaging gradient. We obtained linewidths of 0.6–1.5 Hz for all the experiments by shimming directly on the polarized ^{129}Xe gas samples.

Three pulse sequences used in this work are shown in Fig. 2. In the pulse sequence used for imaging [Fig. 2(a)], the

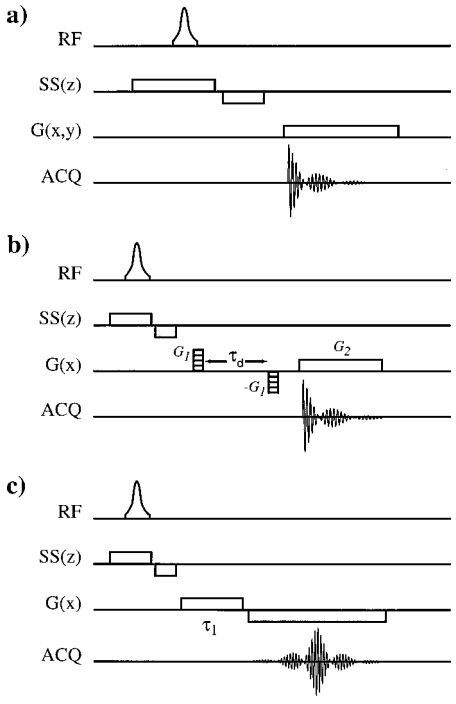

FIG. 2. Pulse sequences used for the three sets of experiments. (a) The rf pulse is a Gaussian amplitude-modulated pulse of 500 μs and is applied during a slice selection gradient (SS) along **z**. The imaging gradient was applied along either **x** or **y** depending on the experiment. (b) The pulse sequence for the measurement of the displacement distribution in the xenon gas sample. The displacement dimension is formed by stepping the gradient strength G_1; the second gradient is equal to the first gradient in strength but opposite in sign. The second dimension originates from direct imaging with the gradient G_2. (c) The pulse sequence used in the edge-enhancement imaging experiments. Imaging gradients were along **x**; the duration τ_1 of the first gradient was varied.

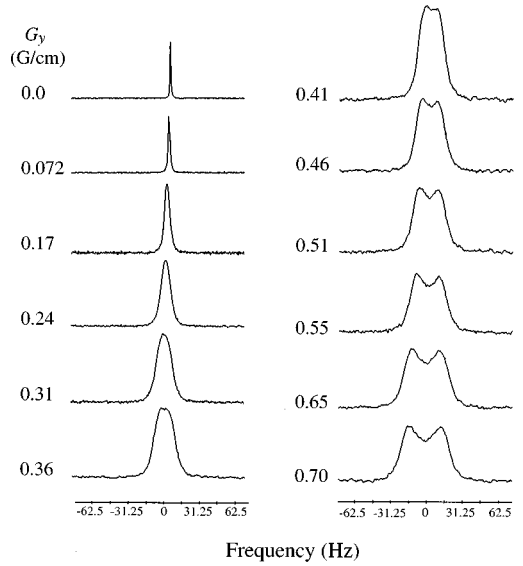

FIG. 3. ^{129}Xe NMR spectra as a function of applied gradient along **y**, obtained with $G_y = 0$, 0.072, 0.17, 0.24, 0.31, 0.36, 0.41, 0.46, 0.51, 0.55, 0.65, and 0.70 G/cm. These images depict the evolution of the line shape with increasing gradient in the strong-diffusion regime.

excitation is achieved with a 500 μs Gaussian pulse applied during a slice-selection gradient along **z**. The tipping angle of this excitation pulse was less than 5°. Following the excitation pulse, a field gradient pulse is applied, and the signal is acquired and Fourier transformed to obtain the image. Next, the displacement distribution measurements were performed using the pulsed-field-gradient spin-echo method.[18] The pulse sequence used in this experiment is shown in Fig. 2(b), where the displacement dimension is formed by incrementing the strength of the gradient G_1, with the second dimension originating from acquisition under the gradient G_2. The sequence measures the distribution of displacement as a function of position. In these experiments, both G_1 and G_2 were gradients along **x**. The slice-selected excitation used for this experiment is the same as that in the imaging experiments described above. Finally, the pulse sequence utilized for edge-enhanced imaging is shown in Fig. 2(c). In performing these experiments, both imaging gradients were along **x** and the duration τ_1 of the first gradient was varied.

All experiments were performed on a Chemagnetics Infinity spectrometer (Otsuka Electronics) and a Quest 4300 spectrometer (Nalorac Cryogenics) at a magnetic field of 4.3 T. A home-built probe was used with a commercial microimaging gradient set (Nalorac Cryogenics). Isotopically enriched (80% ^{129}Xe, Isotec) was used in all experiments. The optical pumping technique and apparatus used to generate polarized xenon have been described in previous publications.[19]

III. RESULTS AND DISCUSSION

A. One-dimensional imaging

A series of 1-D images was taken as a function of the gradient G. Two sets of images are shown, respectively, in Fig. 3 for G along **y** and in Fig. 4 for G along **x**. Adjustment of the gradient direction was performed in order to avoid

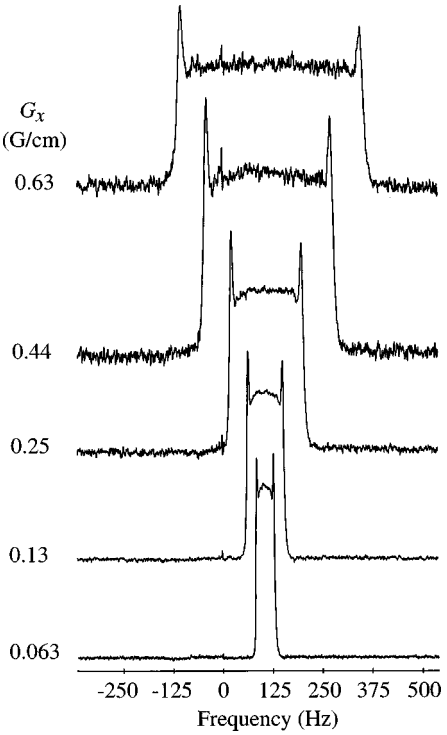

FIG. 4. ^{129}Xe NMR spectra as a function of applied gradient along **x**, obtained with $G_x = 0.063$, 0.13, 0.25, 0.44, 0.63 G/cm. These images depict the evolution of the line shape with increasing gradient in the weak-diffusion regime.

extra broadening and line shape distortion. This was particularly serious when the gradient was applied along **y** because of the geometry of the sample; a 2° error in the gradient vector direction caused severe distortion of the lineshape, completely masking the effects of diffusion at low gradient strength. Eight images are shown in Fig. 3 with G along **y** and a gradient range of 0–0.70 G/cm. These images display a smooth evolution of the line shape from a sharp resonance at zero gradient, to a slightly broadened but still single resonance at small gradient, to the development of two broad lines at higher gradient strength.

A second set of five images is shown in Fig. 4 where G is along **x** and the gradient range is 0.063–0.63 G/cm. The image intensity becomes rather flat in the middle region of the image and one can observe that the two broad features seen in the previous images of Fig. 3 have developed into sharp, well-defined spikes corresponding to positions near the edges of the sample. One may also notice a slight but obvious drop in intensity just inside each of the two spikes, as predicted in previous theoretical work.[8,9,13] Qualitative observations of such edge spikes in polarized gas samples have been reported earlier;[16,20] in fact, Saam *et al.*[16] used this effect to demonstrate edge enhancement in the images of polarized ^{3}He gas samples. There is, however, no previous demonstration of strongly diffusion-averaged images such as those shown in Fig. 3.

A conceptual understanding of these diffusion-mediated image distortions is straightforward, at least at the extremes of weak and strong diffusion. A parameter that characterizes these two regimes has been introduced by de Swiet and Sen[13]

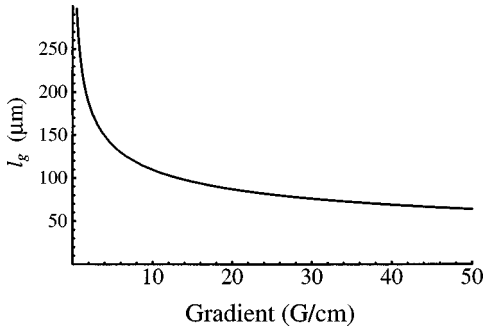

FIG. 5. A plot of l_g vs gradient strength over the range of a typical MRI spectrometer, for xenon gas pressure of 1 atm. The limit of the MRI resolution is approximately $2l_g$.

$$l_g = \sqrt[3]{\frac{D}{\gamma G}}, \tag{1}$$

where D is the diffusion coefficient of the substance, γ is the gyromagnetic ratio of the nuclear spin, and l_g is defined as the diffusion length. l_g determines the distance that a molecule will diffuse in the amount of time that its nuclear spins acquire a unit of phase under a gradient of strength G. A plot of l_g vs G is shown in Fig. 5 for xenon gas over the range of the gradient strength of a typical MRI spectrometer. The maximum imaging resolution is limited to about $2l_g$; for this reason the resolution obtainable from xenon gas imaging is limited to about 100 μm for a typical gradient value in a micro-imaging apparatus at one atmosphere of xenon pressure.

When l_g is much greater than the geometric dimension l_s of the sample along the direction of the gradient vector (strong-diffusion regime), a spin will travel throughout the available space before the dephasing from the gradient can occur. In this case an averaged frequency of the nuclear spin is measured. All of the spins have essentially lost their memory of their initial positions; thus all have the same average frequency giving rise to a single resonance line, as shown in the first four spectra of Fig. 3. In this regime the effect of the gradient is primarily manifested by an apparent broadening of the resonance linewidth. As shown in previous theoretical work,[13] the shape of the resonance can be approximated by a Lorentzian. Indeed, Lorentzian line shapes are clearly manifested in the first three images in Fig. 3. The Lorentzian line shapes of the signals originate from the rapid motion of xenon during the application of the magnetic field gradients; in fact, de Swiet[14] has shown that the Lorentzian line shape persists up to $l_s/l_g = 2$. In this regime, an analytical expression for the time dependence of the NMR signal $S(t)$ is given in Ref. 21

$$\frac{S(t)}{S(0)} = \exp\left(-t \cdot \frac{\gamma G l_s^4}{120 \cdot l_g^3}\right) \tag{2}$$

and the corresponding frequency domain line shape is given in Ref. 14. In Fig. 6 we compare the above theoretical results for $1/T_2^* \equiv \gamma G l_s^4/(120 \cdot l_g^3)$ with our experimental values from the initial slope of the signal decay. Our data matches the

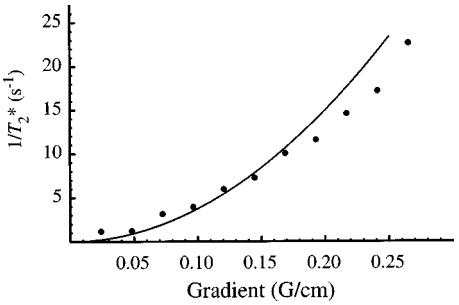

FIG. 6. A plot of $1/T_2^*$ as a function of G. Filled circles are from the time-domain data taken in the strong-diffusion regime, with the contribution from the residual field inhomogeneity removed by subtracting the value of $1/T_2^*$ when $G=0$. The curve was calculated using Eq. (2). Experimental values deviated from the theory when $G>0.17$ G/cm due to the departure from Lorentzian line shape.

theoretical prediction quantitatively for $G \leqslant 0.17$ G/cm; the deviation at higher gradients is due to the departure from a Lorentzian line shape.

When $l_g \ll l_s$ (weak-diffusion regime), the effects of diffusion are most clearly observed near the edges (where diffusive motion is restricted). This effect can be understood qualitatively in the following manner. Because xenon atoms near the edges of the sample are reflected back upon collision with the edges, the average displacement of these xenon atoms is smaller than the displacement of the xenon atoms in the middle of the sample during the application of the gradient. Thus the decay of the signal near the edges is slower than in the middle. This slower decay in the time-domain signal causes the pronounced, narrow spikes to appear near the edges in the images of Fig. 4. In addition, the reflection at the edges also leads to each peak being positioned at some distance ($\sim l_g$) from the actual edge. It can be shown theoretically[14] that this distance is equal to $-a_1' l_g$, where a_1' is the first zero of the derivative of the first Airy function, and $a_1' \approx -1.0188$: This value is consistent with our results and with those of Saam *et al.*[16] It is important to notice that such amplitude variations are only relative and the integral of the image is conserved regardless of the diffusion in the sample. An analytical solution of the diffusion problem in one dimension has been reported[12,14] and it was shown[14] that the peaks near the edges can be identified with slowly relaxing normal modes.

In order to compare our experimental observations with theory, we performed numerical simulations of the diffusion of xenon in our 1D sample in the presence of magnetic field gradients. In these simulations, we modeled xenon diffusion by allowing dimensionless particles to make random walks between the boundaries, and then followed the phase accumulation as a function of time. The simulated free-induction-decay signals were then Fourier transformed to obtain images. Up to one million particles were used in order to reduce the noise in the simulations. The algorithm for our simulation is similar to those used by Hyslop and Lauterbur[8] and Putz *et al.*,[9] and our results agree with these reports given the same set of parameters. Three of these simulated images are shown in Fig. 7 together with the experimental images obtained at the corresponding gradient values. The simulations

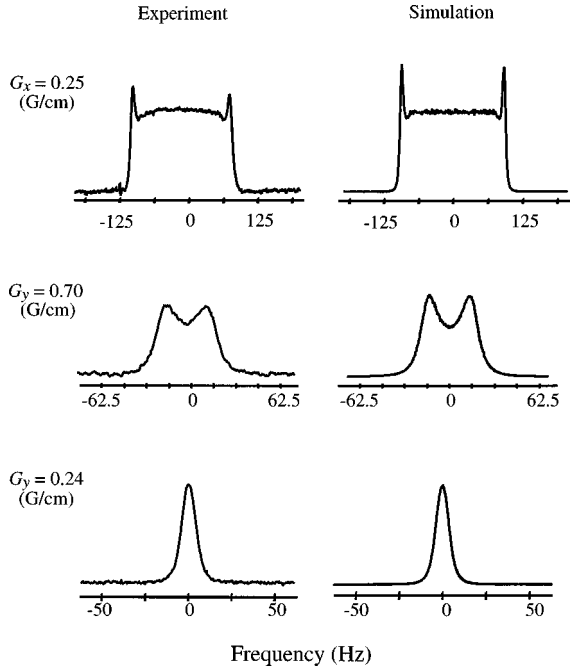

FIG. 7. Comparison of experimentally obtained images with numerical simulations. 1-D simulations were performed for the images obtained with gradient strengths of 0.24 and 0.70 G/cm along y and 0.25 G/cm along **x**.

reproduce the experimental results well in all three cases. The principle sources of peak asymmetry in these images are likely to have been inhomogeneity in the static magnetic field and imperfections in the sample geometry.

B. Measurements of the displacement distributions

As previously discussed, the different diffusion behavior near the boundaries and the center of the sample is due to the impermeability of the glass walls. Very close to the walls, the xenon can only diffuse inward and thus the distribution of the displacement is changed compared to the xenon atoms near the center of the sample. Such a change in displacement distribution gives rise to two effects: (a) a net displacement of the gas atoms near the edges towards the center; (b) the range of the displacement for atoms near the edges is reduced. In fact, effects (a) and (b) correspond, respectively, to the first and second moments of the displacement distribution, which is a Gaussian for diffusion in free space. However, at the edges, the distribution is neither Gaussian nor symmetric and thus higher order moments are also significant. Thus, it is useful to characterize such behavior by directly measuring the displacement distribution as a function of position in the sample. For example, by measuring the displacement distribution, one could obtain a spatially dependent diffusion constant whose values are expected to be larger in the middle of the sample and smaller near the edges.[22]

The displacement distribution was measured using the pulse sequence shown in Fig. 2(b); the time domain data were Fourier transformed in both dimensions, as shown in

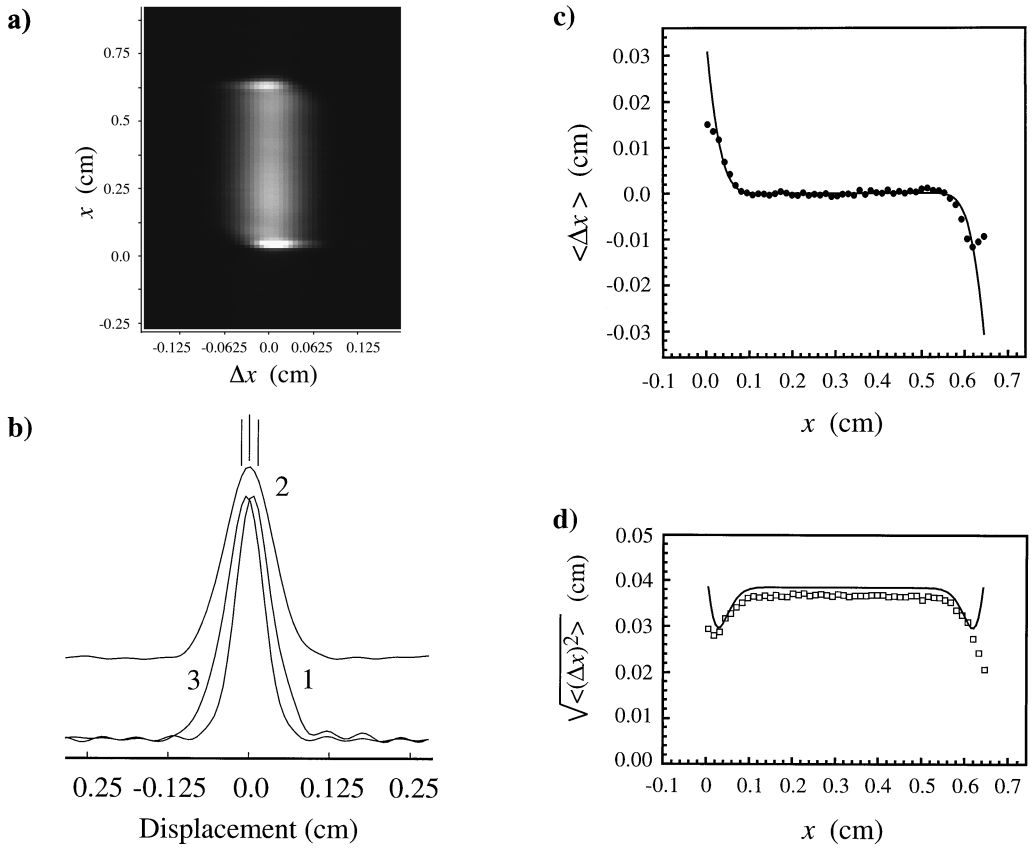

FIG. 8. (a) Measurement of the displacement distribution as a function of position along **x** at $\tau_d = 25$ ms acquired with the pulse sequence shown in Fig. 2(b). Differences in the displacement distribution caused by constrained diffusional motion near the sample boundaries are evident. (b) Normalized displacement distribution near the two edges (slices 1 and 3) and in the center (slice 2). The lines indicate the mean displacement for each distribution. (c) Plot of the mean displacement (first moment) as a function of x. Filled circles are data calculated from (a), and the curve represents theoretical values from Eq. (4), experimental data were shifted up ≈ 23 μm to correct for a slight deviation from zero due to gradient mismatch. The net displacement of the xenon atoms near the two edges toward the center is clearly shown. (d) Plot of the range of displacement (second moment) as a function of x. Open squares are data calculated from (a), and the curve represents theoretical values from Eq. (5). A decrease in diffusive motion is manifested near the edges; however, the growth at the edges shown in the theoretical values was not observed experimentally due to insufficient resolution.

Fig. 8(a). When normalized, this figure shows the probability $P(x,x_0,t)$ of displacement $x-x_0$ as a function of the starting position x_0 over a time period t. Because xenon atoms at the edges can only diffuse inward, one would expect that the displacement distributions at the two edges would slant toward opposite directions, while the displacement distribution at the center of the sample would be symmetrical. Indeed, Fig. 8(a) demonstrates just such behavior; due to the finite resolution of the imaging along **x**, the slanting of the distribution is blurred and rather weak, but still observable. The displacement distribution at the two edges and the center is shown in Fig. 8(b). In this figure it is clear that the distributions at both edges are asymmetric and skew toward opposite directions. Values of both the mean displacement and the second moment of the displacement distribution were calculated for all slices from the data in Fig. 8(a), and are shown in Figs. 8(c) and 8(d), respectively. The net displacement toward the center of xenon near the edges, as well as a decrease in the range of diffusive motion near the edges, is clearly observable.

One may analytically solve the diffusion equation near a one-dimensional wall using a Green's-function approach and obtain the probability of finding an atom at a position x after diffusing from the original position x_0 over a time t

$$P(x,x_0,t)=\frac{1}{\sqrt{4\pi Dt}}\{\exp[-(x-x_0)^2/4Dt] + \exp[-(x+x_0)^2/4Dt]\}. \tag{3}$$

The position of the wall is defined to be at $x=0$. For regions sufficiently far from the wall, $x \gg \sqrt{2Dt}$, this function reduces to the familiar Gaussian form for diffusion in free space. Since the sample dimension is much longer than $\sqrt{2Dt}$, the effect of the other edge is negligible and it is sufficient to consider one edge alone. The average displacement and the width of the displacement distribution can be calculated using Eq. (3)

$$\frac{\langle \Delta x \rangle}{d}=\sqrt{\frac{2}{\pi}}\left\{\exp\left(-\frac{x_0^2}{2d^2}\right)+\frac{x_0}{d\sqrt{2}}\left[\operatorname{erf}\left(\frac{x_0}{d\sqrt{2}}\right)-1\right]\right\}, \tag{4}$$

$$\frac{\langle(\Delta x)^2\rangle}{d^2}=1-\sqrt{\frac{8}{\pi}}\cdot\frac{x_0}{d}\exp\left(-\frac{x_0^2}{2d^2}\right)+\frac{2x_0^2}{d^2}\times\left[1-\mathrm{erf}\left(\frac{x_0}{d\sqrt{2}}\right)\right], \quad (5)$$

where $d=\sqrt{2Dt}$ and $\Delta x=x-x_0$. Plots of the calculated $\langle\Delta x\rangle$ and $\sqrt{\langle(\Delta x^2)\rangle}$ values are shown along with the experimentally measured data in Figs. 8(c) and 8(d).

C. Edge-enhanced imaging

Diffusion-weighted imaging has been utilized in many areas of magnetic resonance imaging.[1,23,24] In fact, it has been suggested that the effects of diffusion can be used to detect impermeable and semipermeable membranes.[8] As previously mentioned, it has been shown that diffusion-mediated edge spikes like those seen in Fig. 4 can be used to differentiate between the boundaries and bulk of a sample of polarized gas, and thus represent a form of edge enhancement.[16] However, such contrast between the edge and bulk signals can be greatly increased by the application of a pulse sequence that takes advantage of the different behavior of the diffusion in these regions. In the case of our 1D sample, one may understand such an ''active'' edge-enhancement method in terms of a position-dependent diffusion constant, $D(x)$. According to the displacement distribution, $D(x)$ would be smaller near the boundaries; thus the decay of the NMR signals during the application of a magnetic field gradient should be slower near the boundaries and faster in the center. The contrast between the boundaries and the interior of the sample should therefore become more pronounced if sufficient time is allowed for diffusion to occur during the pulse sequence.

In order to demonstrate such edge-enhanced imaging, we employed the pulse sequence depicted in Fig. 2(c). Images shown in Fig. 9 were taken with $\tau_1=2$, 4, 6, 8, 10 ms. For $\tau_1=2$ ms, the diffusion is not significant enough to change the ratio of the signals from the edges and the center of the sample, and an essentially static image was obtained. When $\tau_1\geqslant 4$ ms the effect of diffusion is easily discernible in that the signal intensity corresponding to the edges is stronger than the intensity corresponding to the middle of the sample. At $\tau_1>6$ ms the signals originating from the center of the sample are almost negligible, and only the xenon near the edges of the sample contributes to the images. This same effect has been observed in the experiments of of Callaghan *et al.*[11] using ^{1}H MRI.

While this simple imaging sequence can produce high contrast between the boundaries and the interior of a sample, this is accomplished at the expense of the signal intensity. For example, the signal-to-noise ratio for the $\tau_1=8$ ms image is approximately two orders of magnitude less than that for the $\tau_1=2$ ms image. Even with the use of polarized xenon, some signal averaging was performed in order to obtain the $\tau_1=8$ and 10 ms images.

It is intuitively appealing to consider the model of a position-dependent diffusion constant in order to explain the behavior of the images obtained in Fig. 9, including the effects of the net displacement of xenon near the edges. However, such a model does not correctly describe the functional form of the signal decay for the edges at long times. As pointed out by de Swiet,[14] the decay of the signal S at the peaks near the edges changes from a τ_1^3 dependence ($\log(S)\propto-\tau_1^3$), to one that is linearly dependent on time ($\log(S)\propto-\tau_1$). This change in the functional form naturally results in a much extended signal at long times, and hence produce sharp peaks in the images near the sample's edges following Fourier transformation. This exponential time dependence also explains why there is little change in the width of the edge peaks in the images for $\tau=6,8,10$ ms as a function of time.

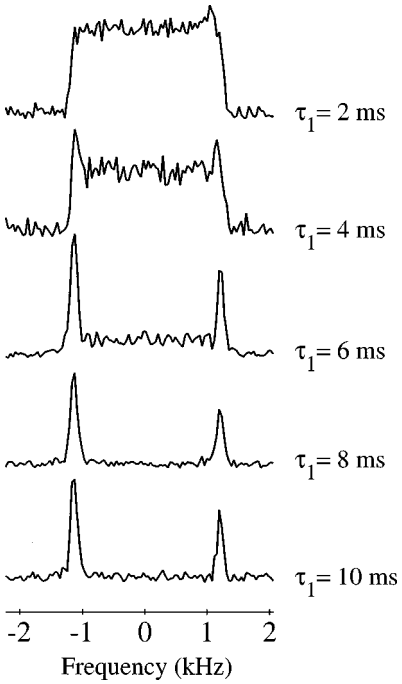

FIG. 9. Edge-enhanced imaging. Images were obtained using the pulse sequence shown in Fig. 2(c), with τ_1 values of 2, 4, 6, 8, and 10 ms and a gradient of 3.3 G/cm along **x**. The images taken with $\tau_1=8$ and 10 ms were acquired with 90° excitation pulses and 32 and 64 averages, respectively; the recycle delay was long enough to allow the diffusion in the sample to replenish the polarized xenon in the space being imaged. Restricted diffusion at the edges of the sample reduces the decay of signal suffered in the middle of the sample. The asymmetry in peak heights from the sample edges is most likely due to inhomogeneity in the static magnetic field and contributions from imperfections in the sample's geometry.

IV. CONCLUSION

We have characterized the effects of diffusion on MR images in one dimension in both the weak and strong-diffusion regimes. Our results agree with previous theoretical and experimental work. Measurements of the displacement distribution were used to depict the behavior of diffusion in different regions of the sample; furthermore, it was shown that this behavior could be used to greatly enhance the contrast between the sample's edges and bulk during MRI. Boundary detection schemes that take advantage of diffusion, in addition to studies of boundary-constrained diffusional motion, may have application to medical and materials imaging using polarized noble gases.

ACKNOWLEDGMENTS

The authors wish to thank Professor P. T. Callaghan, Professor P. C. Lauterbur, and Dr. B. Saam for helpful discussions, and T. Lawhead for his expert glass-blowing and advice. Y.-Q.S. and T.d.S. acknowledge research fellowships from the Miller Institute for Basic Research in Science. This work was supported by the Director, Office of Basic Sciences, Materials Sciences Division of the U.S. Department of Energy under Contract No. DE AC03-76SF00098.

[1] For review see: F. W. Wehrli, Prog. NMR Spectrosc. **28**, 87 (1995).
[2] M. S. Albert, G. D. Cates, B. Driehuys, W. Happer, B. Saam, C. S. Springer, Jr., and A. Wishnia, Nature (London) **370**, 199 (1994).
[3] P. Bachert, L. R. Schad, M. Bock, M. V. Knopp, M. Ebert, T. Großman, W. Heil, D. Hofmann, R. Surkav, and E. W. Otten, Magn. Reson. Med. **36**, 192 (1996).
[4] J. R. Macfall, H. C. Charles, R. D. Black, H. Middleton, H. J. C. Swartz, B. Saam, B. Driehuys, C. Erickson, W. Happer, G. D. Cates, G. A. Johnson, and C. E. Ravin, Radiology **200**, 553 (1996).
[5] M. Ebert, T. Großmann, W. Heil, W. E. Otten, R. Surkau, M. Leduc, P. Bachert, M. V. Knopp, L. R. Schad, and M. Thelen, Lancet **347**, 1297 (1996).
[6] J. P. Mugler III, B. Driehuys, J. R. Brookeman, G. D. Cates, S. S. Berr, R. G. Bryant, T. M. Daniel, E. E. del Lange, J. H. Downs III, C. J. Erickson, W. Happer, D. P. Hinton, N. F. Kassel, T. Maier, C. D. Phillips, B. T. Saam, K. L. Sauer, and M. E. Wagshul, Magn. Reson. Med. **37**, 809 (1997).
[7] Y.-Q. Song, H. C. Gaede, T. Pietraß, G. A. Barrall, G. C. Chingas, M. R. Ayers, and A. Pines, J. Magn. Reson., Ser. A **115**, 127 (1995).
[8] W. B. Hyslop and P. C. Lauterbur, J. Magn. Reson. **94**, 501 (1991).
[9] B. Putz, D. Barsky, and K. Schulten, J. Magn. Reson. **97**, 27 (1992).
[10] D. Barsky, B. Putz, K. Schulten, J. Schoeniger, E. W. Hsu, and S. Blackband, Chem. Phys. Lett. **200**, 88 (1992).
[11] P. T. Callaghan, A. Coy, L. C. Forde, and C. J. Rofe, J. Magn. Reson., Ser. A **101**, 347 (1993).
[12] S. D. Stoller, W. Happer, and F. J. Dyson, Phys. Rev. A **44**, 7459 (1991).
[13] T. M. de Swiet and P. N. Sen, J. Chem. Phys. **100**, 5597 (1994).
[14] T. M. de Swiet, J. Magn. Reson., Ser. B **109**, 12 (1995).
[15] P. W. E. Peereboom, H. Luigjes, and K. O. Prins, Physica A **156**, 260 (1989).
[16] B. Saam, N. Drukker, and W. Happer, Chem. Phys. Lett. **263**, 481 (1996).
[17] D. M. Schmidt, J. S. George, S. L. Penttila, A. Caprihan, and E. Fukushima, J. Magn. Reson. **129**, 184 (1997).
[18] J. Karger and W. Heink, J. Magn. Reson. **51**, 1 (1983).
[19] D. Raftery, H. Long, T. Meersmann, P. J. Gradinetti, L. Reven, and A. Pines, Phys. Rev. Lett. **66**, 584 (1991); H. C. Gaede, Y.-Q. Song, R. E. Taylor, E. J. Munson, J. A. Reimer, and A. Pines, Appl. Magn. Reson. **8**, 373 (1995).
[20] R. E. Taylor, Y.-Q. Song, T. R$\tilde{o}\tilde{o}$m, S. Appelt, R. Seydoux, A. Bifone, D. de Graw, B. Goodson, D. Laws, and A. Pines, 37th Experimental Nuclear Magnetic Resonance Conference, Pacific Grove, CA, 1996.
[21] R. C. Wayne and R. M. Cotts, Phys. Rev. **151**, 264 (1996).
[22] The second moment of the displacement distribution actually becomes wider *at* the edges [see Fig. 8(d)]; therefore, any calculated position-dependent diffusion constant would become larger at these points. However, due to limited spatial resolution in our experiment, it is difficult to directly observe this phenomenon.
[23] D. Le Bihan, E. Breton, D. Lallemand, P. Grenier, E. Cabanis, and M. Laval-Jeantet, Radiology **161**, 401 (1986).
[24] R. Turner and D. Le Bihan, J. Magn. Reson. **86**, 445 (1990).